

Barkhausen pulse structure in an amorphous ferromagnet: Characterization by high-order spectra

J. R. Petta and M. B. Weissman

Department of Physics, University of Illinois at Urbana-Champaign, 1110 West Green Street, Urbana, Illinois 61801-3080

Gianfranco Durin

Istituto Elettrotecnico Nazionale Galileo Ferraris and INFM, Corso Massimo d'Azeglio 42, I-10125 Torino, Italy

(Received 22 October 1997)

Frequency-dependent third and fourth moments of the Barkhausen signal from a soft amorphous ferromagnet are measured. The data indicate strong coupling between the power in different frequency bands. The sign of the time asymmetry of a third-order voltage correlation indicates that the high-frequency Barkhausen events, on average, systematically precede the low-frequency Barkhausen events. The results are inconsistent with several commonly employed models. [S1063-651X(98)10205-2]

PACS number(s): 05.40.+j, 75.60.Ej

INTRODUCTION

Since its discovery, the Barkhausen effect has proven useful in the study of domain wall dynamics in soft ferromagnetic materials. The simplest early models described Barkhausen jumps as individual events of the same magnitude, duration, and shape, Poisson distributed in time [1]. More plausible models [2,3] allow for distributions of pulse durations and heights. In such models it is often simply assumed that the spectral density $S_1[f_1]$ comes primarily from pulses whose width is about $1/f_1$ [2-4], giving simple mathematical relations among scaling laws for the pulse duration, frequency of occurrence, height, and $S_1[f_1]$ [5]. In contrast, the model of Alessandro *et al.* (designated ABBM) [6] describes the motion of a domain wall characterized by a single position moving over a spatially varying coercive field. There have long been suggestions [7] that the domain wall motions are self-organized, meaning that the noise statistics would be determined by self-consistent properties of many interacting domain-wall segments, rather than directly by the statistics of separately pinned domains or of the underlying coercive field. Recently some papers, e.g., [8], have claimed evidence for self-organized criticality.

So far, the most detailed successful experimental predictions have come from the ABBM model [9,10], applied to soft magnetic metals, but in its original formulation, that model invoked physically unrealistic extended spatial correlations in the coercive field [11]. Recent experiments indicate that a correct physical picture of domain wall dynamics must include coupling between neighboring segments of domain wall and/or other domains [11,12]. Progress has now been made toward constructing a model of a flexible domain wall including long-range magnetic dipole interactions [12,13], with the ABBM picture emerging in some limits as an effective theory for the net magnetization changes rather than as a direct picture of a single domain-wall position [14]. No model has yet been able to clarify the variability of the high-frequency power spectrum exponent, which experimentally ranges between 1.5 and 2 [15].

In this paper we explore several relevant questions using frequency-dependent third and fourth moments of the

Barkhausen signal. How the spectral shape (and exponent, if one exists) is to be determined from any model depends on whether the high-frequency noise power comes primarily from short pulses or from fine structure on long pulses, i.e., whether the common analysis in terms of distributions of parameters of elementary events is applicable. Our key test of the hypothesis that the form of $S_1[f_1]$ is determined by the distribution of the pulse widths will be whether the time-dependent spectral power at high frequencies fluctuates independently of the spectral power and of the voltage at much lower frequencies. We also look for time-asymmetric higher-order voltage correlations, to specifically check a prediction (derivable from the ABBM model or from any model that is strictly mathematically equivalent to it) that all such moments are symmetrical [16]. In the models invoking interacting parts of a domain wall, the statistical properties (including any semblance of self-organized criticality) depend strongly on the demagnetizing effect [12-14], which in turn depends strongly on the geometry of the sample. We investigate the dependence of the connection of events on different time scales on these long-range effects by altering the overall permeability of the sample with a magnetic yoke.

STATISTICAL TOOLS

It is useful to define some statistical tools used to analyze a time series $\{v[t_i], 0 \leq i \leq 2^m - 1\}$, where $t_i - t_{i-1} = 1/f_s$, with f_s being the sampling frequency. We use a running time average of the voltage over different time scales:

$$V_n(j) \equiv \sum_{i=2^n j}^{2^n(j+1)-1} v(t_i) \quad \text{for } 0 \leq n < m$$

$$\text{and } 0 \leq j \leq 2^{m-n} - 1. \quad (1)$$

In other words, we average 2^n points to get a sequence of voltages with an effective sampling rate of $f_s/2^n$. This running average then is useful in generating a Haar transform. The Haar transform has an advantage over the Fourier transform $F(v)$ [used to generate the ordinary power spectrum $S_1(f_1)$] in that the Haar transform gives up unused frequency

resolution in exchange for improved time resolution, allowing one to keep better track of how the power in some frequency range varies [16]. We define the Haar power:

$$H_n(j) \equiv [V_n(2j+1) - V_n(2j)]^2 \quad \text{for } 0 \leq j \leq 2^{m-n-1} - 1. \quad (2)$$

In order to express this Haar power in ordinary time-frequency units, we define:

$$H(f_1, t) \equiv H_n(j), \quad \text{where } f_1 = f_s/2^{n+1} \\ \text{and } t = (j+1)2^{n+1}/f_s. \quad (3)$$

This Haar spectrum resembles the Fourier spectrum, except that each point contains Fourier components distributed over a range of a few octaves. Following previous work [17], we define a normalized second spectrum (involving a fourth moment of v) by

$$S_2(f_2, f_1) \equiv F(H(t, f_1))(F(H(t, f_1)))^* / \langle H(t, f_1) \rangle^2. \quad (4)$$

Although it is often convenient to subtract the $S_2(f_2, f_1)$ that would be produced by Gaussian noise, that procedure was unnecessary here due to the highly non-Gaussian nature of the noise. We define another spectrum, involving a third moment of v , useful for showing the connection between pulses on one time scale and power on higher-frequency scales:

$$S_{1.5}(f_2, f_1) \equiv F(v(t))(F(H(t, f_1)))^* / \langle H(t, f_1) \rangle. \quad (5)$$

Several qualitative features of these statistical characterizations directly correspond to properties of the underlying model. In any model in which each pulse has a narrow distribution (on a logarithmic scale) of characteristic rates and the pulses occur independently of each other, $S_2(f_2, f_1)$ will be nearly independent of f_2 , since the pulses contributing to the noise at frequencies f_1 will not have any characteristic rates $f_2 \ll f_1$. Likewise, if the high-frequency tail of $H(f_1)$ primarily comes from distinct short-duration Barkhausen pulses, the correlation coefficient between low-frequency voltage fluctuations and low-frequency fluctuations in high-frequency noise power, i.e., $S_{1.5}(f_2, f_1) / (S_1(f_2)S_2(f_2, f_1))^{0.5}$, will be a strongly decreasing function of f_1/f_2 , since the rapid pulses (duration about $1/f_1$) will be uncorrelated with the longer pulses (duration about $1/f_2$). Thus we will have several tests of the proposition that the power in different frequency ranges comes from separate events.

The ABBM model [6] also makes a simple qualitative prediction. The fundamental differential equation on which it is based can be converted by change of variables (solving for the time derivative of the square root of the domain wall velocity, rather than for that of the velocity itself) into an equation formally identical to that for a massless particle with friction diffusing in thermal equilibrium in a potential well, albeit one with a peculiar shape [16]. All correlation functions involving an even number of time derivatives for any such system must obey time reversal symmetry. In particular, the imaginary part of $S_{1.5}$ must have zero expectation value in any such model.

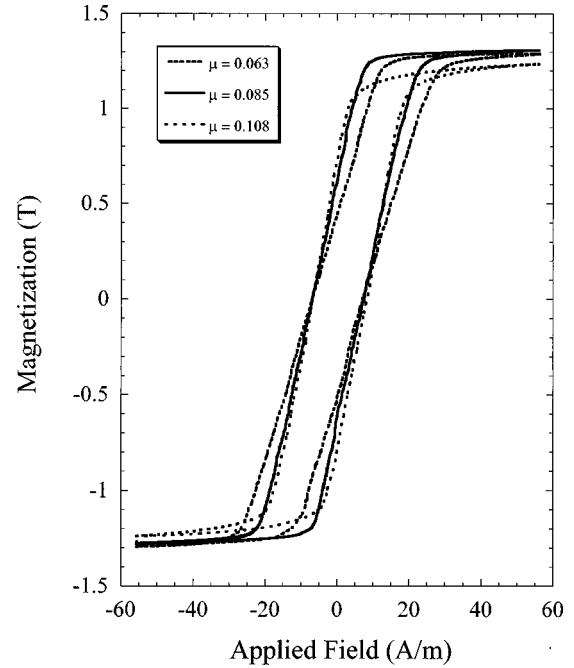


FIG. 1. $\text{Fe}_{21}\text{Co}_{64}\text{B}_{15}$ hysteresis loops for three effective permeabilities, changed by varying the separation between the magnetic yoke and the sample, with the lowest permeability corresponding to no yoke. The maximum applied field in the hysteresis loops corresponds to the maximum applied field during the data acquisition sweeps. Data were acquired only in the linear region of the hysteresis loop.

EXPERIMENTS

The experiments were performed on the as-quenched amorphous alloy $\text{Fe}_{21}\text{Co}_{64}\text{B}_{15}$. Details of $\text{Fe}_{85-x}\text{Co}_x\text{B}_{15}$ sample preparation and characteristics can be found in prior work [15]. The dimensions of the sample ribbon were $20 \text{ cm} \times 0.9 \text{ cm} \times 35 \mu\text{m}$. This sample geometry helps to reduce the effects of the demagnetizing field. The sample has domain walls aligned parallel to the length of the ribbon, with a total of about 50 domain walls. A small pickup coil of 50 turns wrapped around the center of the sample over a 1-mm section detects the Barkhausen noise, while a counterwound air core coil of 50 turns connected in series with the pickup coil offsets the induced voltage from the applied magnetic field. Domain wall motion in the region of the pickup coil induces a voltage in the coil proportional to the sum of the velocities of the domain walls. A 16 cm long solenoid applies the external driving field along the length of the sample. Usually a triangular wave form is used to keep the magnetization rate constant during the data-taking intervals. An adjustable magnetic yoke allows changes in the sample's effective permeability. The entire setup was placed in a mumetal box in a shielded room. Figure 1 shows three hysteresis loops, collected by integrating over the Barkhausen signal, corresponding to three effective permeabilities obtained with different yoke positions.

Driving frequencies for these experiments ranged from 0.01 to 1 Hz, giving values of c (a standard dimensionless parameter describing the magnetization rate, with $c = 1$ at the crossover from a voltage distribution peaked at zero to one peaked at a finite value [6]) ranging from 0.2 to 1. A 12 bit Hewlett Packard analog to digital converter collected 4096-

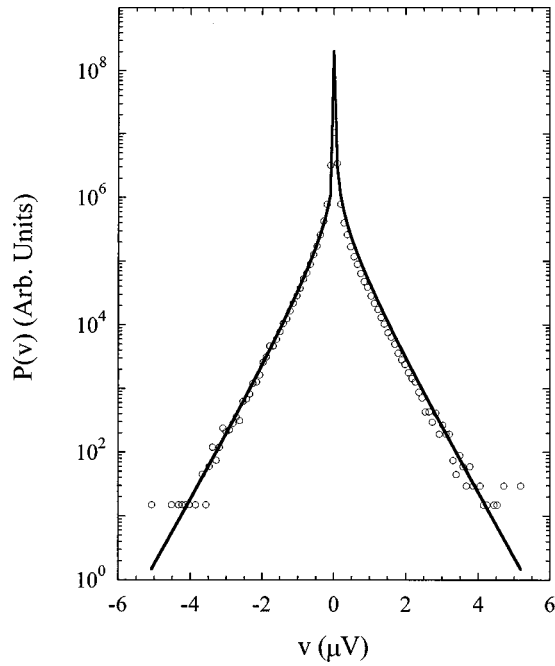


FIG. 2. A domain wall velocity probability distribution curve. The points represent the raw data, while the curve corresponds to the ABBM prediction for $c=0.27$.

point voltage time series, which were then Fourier or Haar transformed and squared to give the power spectrum [16]. All of the data in this article, except for the hysteresis loops, have been averaged over 350 sweeps, corresponding roughly to 85 000 Barkhausen events. The odd-order statistics ($S_{1.5}$) are averaged only over one sign of field sweep. The raw data from $S_{1.5}$ and S_2 were smoothed using a Stineman function [18].

RESULTS

It is convenient to characterize the magnetization rate using the parameter c , which can be determined by comparing the experimental probability density function for the Barkhausen voltage with the predictions of the ABBM model [6], as illustrated in Fig. 2. Figure 3 contains power spectra at three different values of c for $\mu=0.085$. These power spectra and voltage distributions closely resemble those measured previously on similar materials [15]. The dependence of the low-frequency cutoff on c is consistent with predictions of the ABBM model [6].

Figure 4 shows a time series collected for $c=0.7$ and $\mu=0.063$. Qualitatively, the data do not seem to separate cleanly into simple pulses with a single characteristic time associated with each pulse. Our statistical analysis is mainly used to quantify this impression.

Figure 5 shows S_2 for five different f_1 . The data were collected at $c=0.2$ with a permeability of 0.063. For fixed f_1 , $S_2(f_2, f_1)$ peaks near $f_2=15$ Hz, just as $S_1(f_1)$ peaks near $f_1=15$ Hz. At higher frequencies, $S_2(f_2, f_1)$ falls off approximately as $f_1^{-0.35}$ and $f_2^{-0.35}$. This means that the *variance* in the high-frequency power does not come from independent short-duration pulses (which would give S_2 independent of f_2) but rather from events on time scales much longer than $1/f_1$.

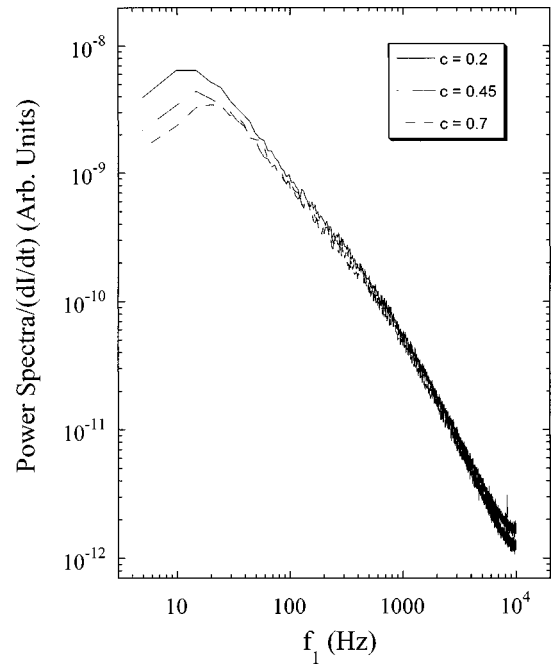


FIG. 3. Power spectra representing three different values of c for $\mu=0.085$ normalized by SI . The low-frequency portion of the power spectra are consistent with the ABBM model, in which an increase in c causes a decrease in the low-frequency power and an increase in the cutoff frequency. $S_1(f_1)$ fall off as $f_1^{-1.2}$ near 100 Hz and as $f_1^{-1.8}$, above 1 kHz. The ABBM model predicts a slope of f_1^{-2} for large f_1 .

The question of how much of the *power* in high frequencies comes from distinct high-frequency pulses rather than from high-frequency structure on low-frequency pulses is not settled by determining that the *variance* comes from such

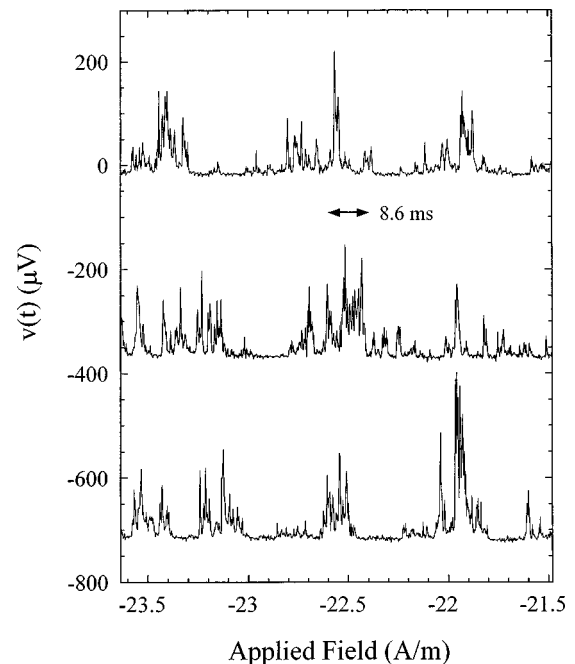


FIG. 4. Three consecutive time series collected for $c=0.7$ and $\mu=0.063$ collected under similar conditions as those used for the higher-order spectral analysis. The long avalanche in the middle sweep has a duration of approximately 8.6 ms.

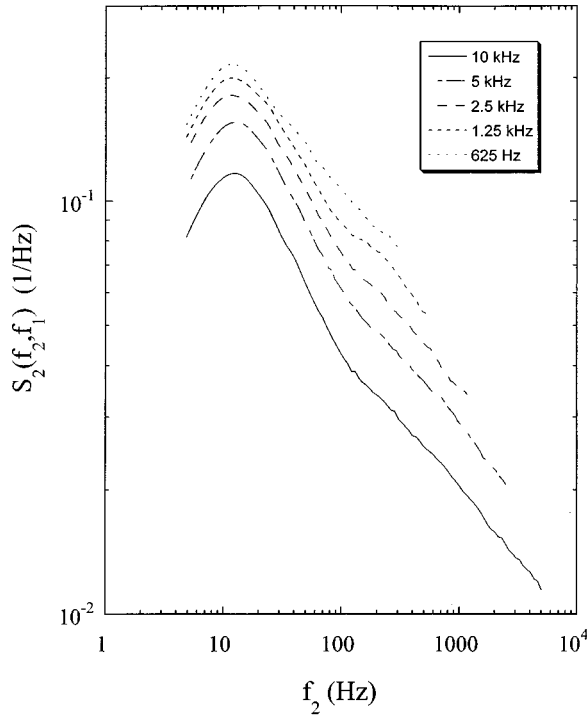


FIG. 5. Normalized second spectra for five f_1 as a function of f_2 . The spectra fall off as $f_1^{-0.35}$ and as $f_2^{-0.35}$. These data were collected for $c=0.2$ and $\mu=0.063$.

structure. This question can be addressed using $S_{1.5}(f_2, f_1)$, shown in Fig. 6 for the same set of data as used in Fig. 5. $S_{1.5}(f_2, f_1)$ depends only weakly on f_1 , indicating that the noise power at high frequencies contains a large tail from

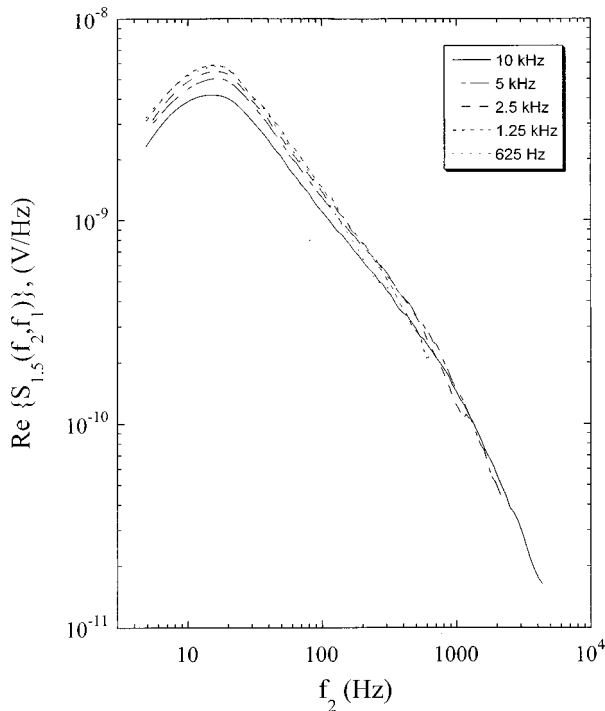


FIG. 6. Normalized 1.5 spectra collected on the same data used for Fig. 5. The spectra show weak dependence on f_1 and fall off as $f_2^{-0.85}$ near $f_1=100$ Hz. The high-frequency exponent is approximately $f_2^{-1.5}$.

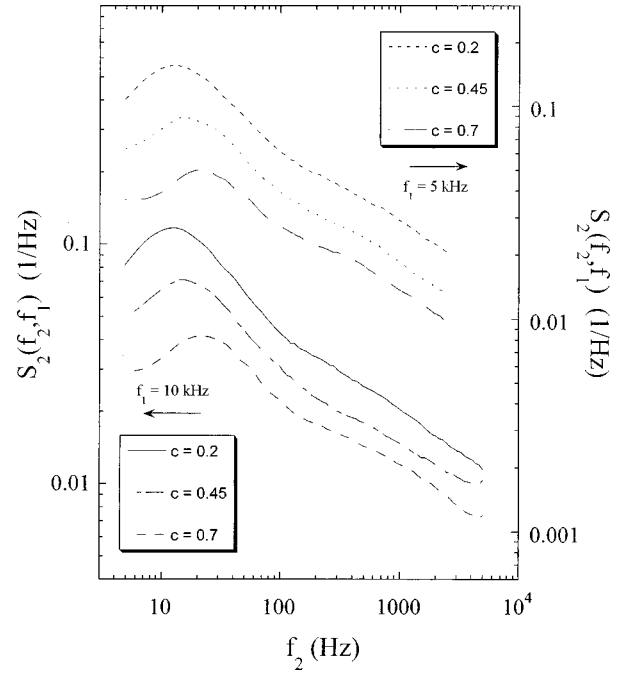


FIG. 7. Normalized second spectra for three different values of c all collected at $\mu=0.085$. Spectra for $f_1=10$ kHz and $f_2=5$ kHz are plotted on separate scales for clarity. The magnitudes of the second spectra and the cutoff frequency are highly dependent on the driving parameter c .

pulses with duration much longer than $1/f_1$. For example, a pulse at 40 Hz contributes almost as much fractional variance to the power at 5 kHz as at 1 kHz, so that it must also contribute nearly as high a fraction of the power at 5 kHz. In order to account for the near independence of $S_{1.5}(f_2, f_1)$ on f_1 , the fraction of the $H(f_1)$ that comes from that tail cannot fall off faster than $f_1^{-0.13}$ in this regime. Given the form of $S_1(f_1)$, about $f_1^{-1.8}$ in this range, that requires that the low-frequency pulses have high-frequency tails that fall off as about $f_1^{-1.8}$ to $f_1^{-1.9}$. As a function of f_2 , $S_{1.5}(f_2, f_1)$ falls off approximately as $f_2^{-0.85}$ near 100 Hz and as $f_2^{-1.5}$ above about 1 kHz, a more dramatic break from simple power-law dependence than found in $H(f_1)$ or $S_1(f_1)$.

The higher-order spectra are altered by changes in the driving frequency. Figure 7 shows $S_2(f_2, f_1)$ for three values of c . An increase in the driving frequency results in the sampling of more pulses, reducing the magnitude of S_2 , since S_2 is normalized to represent fractional fluctuations in power. As c is varied, the low-frequency cutoff of $S_2(f_2)$ changes in just the same way as the low-frequency (f_1) cutoff in $H(f_1)$ or $S_1(f_1)$, as expected if $S_2(f_2, f_1)$ results from structure on $1/f_1$ time scales in pulses of duration $1/f_2$.

By altering the separation distance between the sample and the yoke it is possible to change the effective permeability of the sample. Figure 8 shows $S_2(f_2, f_1)$ for three permeabilities at $c=0.45$. The low-frequency cutoff frequency decreases with increasing μ , as does the cutoff frequency of $S_1(f_1)$. Figure 9 shows the real part of $S_{1.5}(f_2, f_1)$ taken from the same data in Fig. 8, again showing the same low-frequency dependence on μ .

Time asymmetries are easily found by examining the imaginary part of $S_{1.5}(f_2, f_1)$. Figure 10 shows

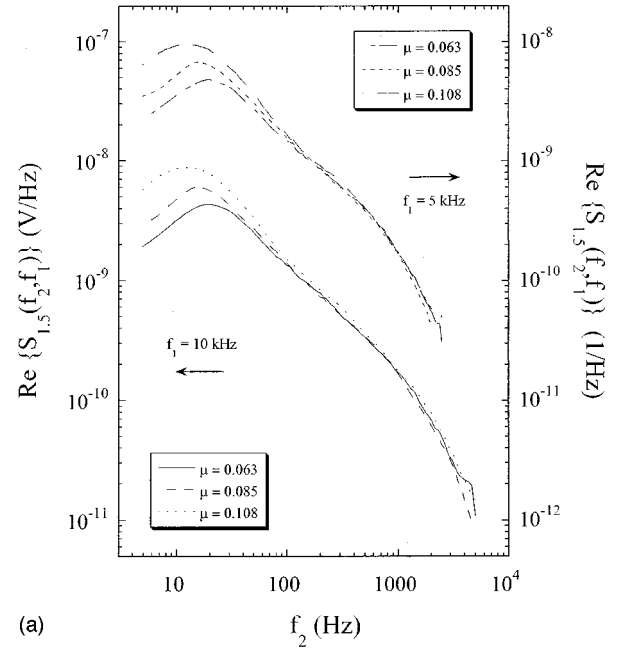
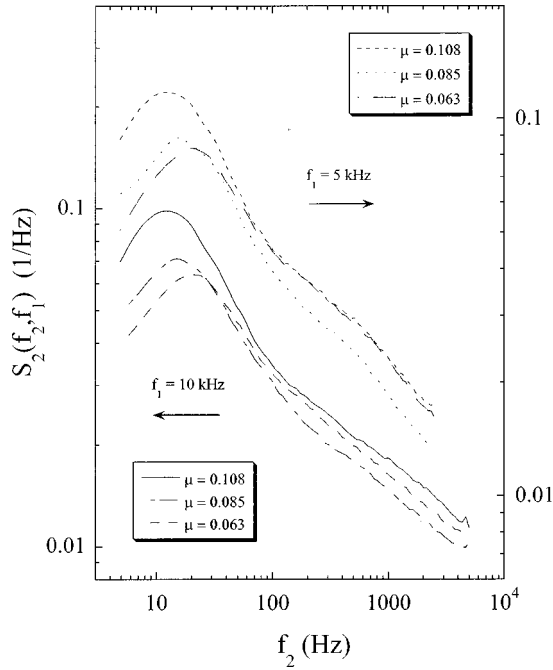


FIG. 8. Normalized second spectra for three different values of μ all collected at $c=0.45$. Spectra for $f_1=10$ kHz and $f_2=5$ kHz are plotted on separate scales for clarity. The low-frequency portion of the spectra and the cutoff frequency are clearly dependent on μ .

$\text{Im}(S_{1.5}(f_2, f_1))/\text{Re}(S_{1.5}(f_2, f_1))$ is generally positive, which indicates (given the sign convention in our program) that, on average, any spurt of low-frequency noise power is preceded by one of high-frequency noise power. $\text{Im}(S_{1.5}(f_2, f_1))/\text{Re}(S_{1.5}(f_2, f_1))$ is an increasing function of f_2 up to frequencies a bit less than f_1 , which means that the time asymmetries arise mostly from asymmetrical structure on individual pulses, rather than from distinct precursor events separated on time scales longer than the pulses themselves. Inspection of Fig. 4 shows some apparent asymmetry of this type, although it is hard to judge reliably by eye without taking the average of the higher-order statistics. $\text{Im}(S_{1.5}(f_2, f_1))/\text{Re}(S_{1.5}(f_2, f_1))$ is nearly independent of the effective permeabilities over the range used in this experiment.

DISCUSSION

Models employing distributions of independent pulses, with the spectral shape determined by the distributions of pulse widths and heights, fail qualitatively to describe the higher-order spectra. The weak dependence of $S_{1.5}(f_2, f_1)$ on f_1 shows that most of the power in the high end of our observed frequency range actually comes from fine structure on the same long pulses giving the low-frequency part of the spectrum. If one nevertheless attempted to formally analyze the data in terms of a distribution of pulse widths and heights, the magnitude of S_2 provides an extra constraint not present when analyzing S_1 alone. The resulting distributions would be unrealistic, e.g., pulse heights that are decreasing functions of width in the 1 kHz regime. Thus a successful model must predict not only the distribution of the pulse widths but also the distribution of frequency components within single pulses.

There are also deviations from the more interesting and

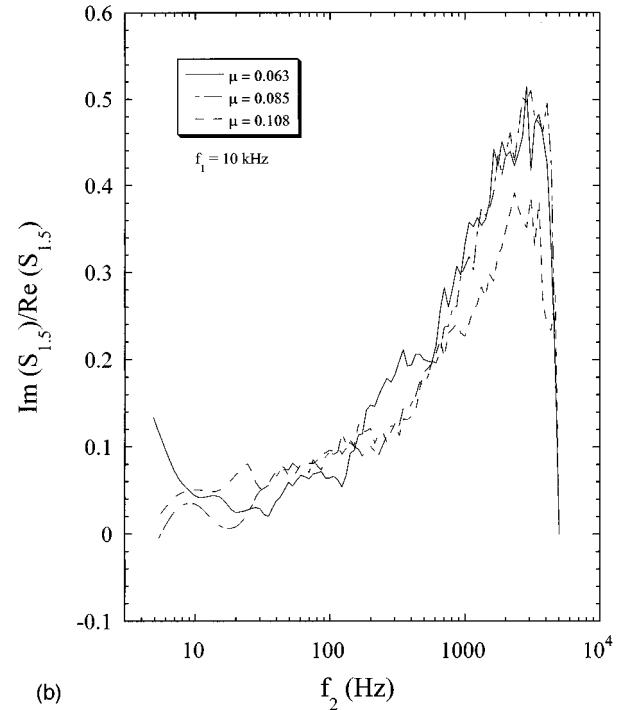


FIG. 9. (a) Normalized 1.5 spectra for three different values of μ taken from the same time series used to calculate the second spectrum in Fig. 8. Spectra for $f_1=10$ kHz and $f_2=5$ kHz are plotted on separate scales for clarity. Again, the low-frequency portion of the spectra and the cutoff frequency are clearly dependent on μ . (b) $\text{Im}(S_{1.5}(f_2, f_1))/\text{Re}(S_{1.5}(f_2, f_1))$ for $f_1=10$ kHz from the same data used in Fig. 8. The positive sign indicates that, on average, low-frequency pulses are preceded by higher frequency pulses. The $\text{Im}(S_{1.5}(f_2, f_1))/\text{Re}(S_{1.5}(f_2, f_1))$ spectra are nearly independent of μ .

generally more successful ABBM model. $V(t)$ in that model is self-affine, i.e., a change of time scale produces a scaling change in voltage scale, above the low-frequency cutoff. The failure of $S_1(f_1)$ to have a single high-frequency scaling exponent already indicates some deviation from that picture, as

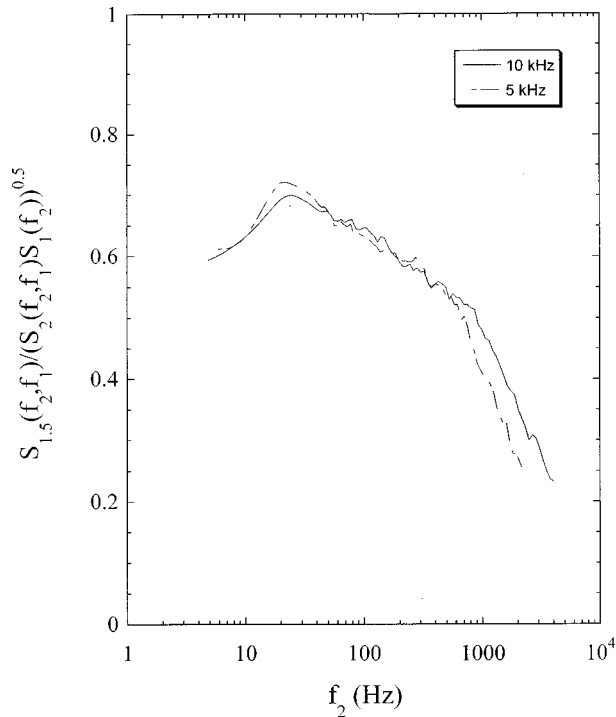


FIG. 10. $S_{1.5}(f_2, f_1) / (S_1(f_2) S_2(f_2, f_1))^{0.5}$ collected for $c=0.2$ and $\mu=0.063$. The correlation coefficient is nearly constant for $f_1 < 600$ Hz and then rapidly decreases above 800 Hz.

has been noted generally for amorphous materials [15]. The existence of strongly time-asymmetric correlation functions (i.e., the imaginary component of $S_{1.5}$) is another qualitative violation of the ABBM picture. Such asymmetries can arise if the effective pinning field is non-Gaussian [16], rather than the Gaussian field assumed in the ABBM picture. It would be interesting to check simulations of interacting domain-wall-segment pictures to see if similar asymmetries appeared in them.

Time-asymmetric higher-order correlations are known to turn up in some self-organized dynamical systems, such as earthquake models with nonlinear local friction [19] or slowly driven sandpiles [20]. The general physical picture of the asymmetries in such models is that small, rapid events smooth the strain distribution, setting the scale for larger, slower events involving more sites. Our results share a general property with many such slowly driven dynamical systems, in that the events on different time scales are closely linked. It would not be correct, however, to describe our results as exhibiting ‘‘self-organized criticality,’’ since there is no extended critical scaling regime of any type in these data.

The correlation coefficient between the low-frequency fluctuations in $V(t)$ and the envelope of high-frequency fluctuations in $V(t)$, i.e., $S_{1.5}(f_2, f_1) / (S_1(f_2) S_2(f_2, f_1))^{0.5}$, shows a particularly sharp deviation from any simple scaling law. This deviation suggests a qualitative interpretation. Most of the noise power in this regime of experimental parameters comes from pulses whose lowest characteristic frequencies range from about 10 Hz to about 1 kHz. In that frequency range, the distribution of pulse widths apparently plays a role in determining the spectral shape, since there is high, nearly constant correlation exhibited in the normalized $S_{1.5}$, as shown in Fig. 10. However, above 800 Hz the correlation coefficient between fluctuations in $V(t)$ and the envelope of higher-frequency fluctuations rapidly falls off.

The apparent meaning is that the noise power at frequencies above a few kHz does not arise from pulses whose lowest characteristic frequency is over 800 Hz. Since there is a break in the scaling of $S_1(f_1)$ near 800 Hz, the most obvious interpretation would be that the spectral shape above that frequency reflects the distribution of Fourier components *within* the longer pulses, rather than the distribution of pulse widths. Although the frequency power law of $S_1(f_1)$ is steeper above 800 Hz than below, extrapolation to the low-frequency cutoff would still indicate that even at 800 Hz more than 30% of the power comes from pulses with lowest characteristic frequency near the low-frequency cutoff.

We conclude that under the conditions of a typical Barkhausen experiment in a soft amorphous metallic ferromagnet, a simple distributed-pulse parameter model does not even approximately capture the relation between events at different frequency scales. The ABBM equations describing a moving domain wall also are inconsistent with some of the statistical features. It remains to be seen what features (e.g., a realistic geometry) are needed in a model of interacting domain wall segments to capture the actual behavior observed, including time asymmetries and strong deviations from scaling.

In contrast to these results, data on single-crystal 3 wt.% Si-Fe (which has a less nearly rectangular hysteresis loop) are much more nearly compatible with an independent-pulse model [21]. Among the factors that might account for this difference are effects connected with the shape of the hysteresis loop [22] and the effect of the lower density of moving domain walls in the FeSi.

ACKNOWLEDGMENTS

J.P. would like to thank the staff of IENGF for making this project possible. This work was supported by NSF Grant No. DMR 96-23478.

- [1] G. Montalenti, *Z. Angew. Phys.* **28**, 295 (1970).
- [2] U. Lieneweg and W. Grosse-Nobis, *Int. J. Magn.* **3**, 11 (1972).
- [3] D. Spasojevic, S. Bukviv, S. Milosevic, and H. E. Stanley, *Phys. Rev. E* **54**, 2531 (1996).
- [4] L. V. Meisel and P. J. Cote, *Phys. Rev. B* **46**, 10 822 (1992).

- [5] H. J. Jensen, K. C. Christensen, and H. C. Fogedby, *Phys. Rev. B* **40**, 7425 (1989).
- [6] B. Alessandro, C. Beatrice, G. Bertotti, and A. Montorsi, *J. Appl. Phys.* **68**, 2901 (1990). The ABBM model defines the dimensionless parameter $c = \dot{I} \sigma G / A \mu$, where \dot{I} is the magne-

- tization rate, σ is conductivity, $G=0.1356$ for typical ribbon geometries, A is a constant (not known independently) proportional to the variance of the effective coercive field, and μ is the permeability.
- [7] T. Erber, S. A. Guralnick, and H. G. Latal, *Ann. Phys. (N.Y.)* **69**, 161 (1971).
- [8] P. J. Cote and L. V. Meisel, *Phys. Rev. Lett.* **67**, 1334 (1991).
- [9] G. Durin, G. Bertotti, and A. Magni, *Fractals* **3**, 351 (1995).
- [10] B. Alessandro, C. Beatrice, G. Bertotti, and A. Montorsi, *J. Appl. Phys.* **68**, 2908 (1990).
- [11] J. R. Petta, M. B. Weissman, and G. Durin, *Phys. Rev. E* **56**, 2776 (1997).
- [12] J. S. Urbach, R. C. Madison, and J. T. Markert, *Phys. Rev. Lett.* **75**, 276 (1995).
- [13] O. Narayan, *Phys. Rev. Lett.* **77**, 3855 (1996).
- [14] P. Cizeau, S. Zapperi, G. Durin, and H. E. Stanley, *Phys. Rev. Lett.* **79**, 4669 (1997).
- [15] G. Durin, A. Magni, and G. Bertotti, *J. Magn. Magn. Mater.* **160**, 299 (1996).
- [16] K. P. O'Brien and M. B. Weissman, *Phys. Rev. E* **50**, 3446 (1994).
- [17] M. B. Weissman, *Annu. Rev. Mater. Sci.* **26**, 395 (1996).
- [18] R. Stineman, *Creative Computing* **16**, 54 (1990).
- [19] B. E. Shaw, J. M. Carlson, and J. S. Langer, *J. Geophys. Res.* **97**, 479 (1992).
- [20] J. Rosendahl, M. Vekic, and J. Kelley, *Phys. Rev. E* **47**, 1401 (1993).
- [21] J. Petta, M. B. Weissman, and G. Durin, *IEEE Trans. Magn.* (to be published).
- [22] J. P. Sethna, K. Dahmen, S. Kartha, J. A. Krumhansl, B. W. Roberts, and J. D. Shore, *Phys. Rev. Lett.* **70**, 3347 (1993).